Earth Planets Space, **57**, 1055–1062, 2005

Strong *S*-wave anisotropy in the aftershock region of the 2000 Tottori-ken Seibu, Japan, earthquake (M_W6.6)

Takeshi Nakamura, Hiroshi Takenaka, and Sadaomi Suzuki*

Department of Earth and Planetary Sciences, Kyushu University, Hakozaki 6-10-1, Fukuoka 812-8581, Japan

(Received January 31, 2005; Revised July 19, 2005; Accepted July 31, 2005)

The 2000 Tottori-ken Seibu earthquake (Mw6.6) occurred in Tottori prefecture, western Japan on October 6, 2000. We conducted aftershock observation and analyzed *S*-wave anisotropy using the aftershocks M_{JMA}2.0 to 3.5 observed at two stations near the aftershock region. The fast *S*-waves are polarized to almost E–W direction, which corresponds to the *P*-axis direction of the mainshock. The delay time of the split *S*-waves ranges between 20 and 100 ms. The crack density inside and outside the aftershock area is estimated from the delay time. The distribution of crack density shows a strong spatial variation and depends on the ratio of the path length inside the aftershock region against the whole path length. Assuming a uniform distribution of anisotropy inside and outside the aftershock region, the crack densities inside and outside are 0.017 and 0.007, respectively. It thus seems probable that in the aftershock region the distribution of cracks is intensive and cracks are opened due to the presence of fluids in seismogenic layers. This considerable spatial variation of anisotropy between inside and outside the aftershock region suggests that the aftershock region may have different mechanical properties from the surrounding area.

Key words: Anisotropy, *S*-wave splitting, cracks, aftershock region, Tottori-ken Seibu earthquake.

1. Introduction

The 2000 Tottori-ken Seibu earthquake M_{JMA}7.3 (Mw6.6 by the National Research Institute for Earth Science and Disaster Prevention) occurred in Tottori prefecture, western Japan on October 6, 2000 (Fig. 1). Many aftershocks occurred, including M_{JMA}5.6 (Mw5.1), in the epicentral area of the mainshock. Most of them were distributed shallower than 15 km in depth. The focal mechanism solution of the mainshock is a strike-slip type (Fig. 1) and the main fault strikes to NNW-SSE with 35 km length (e.g. Ohmi *et al*., 2002; Umeda, 2002). However, despite its large magnitude, the main fault trace did not appear at the surface and hence the basic properties of the fault have not been well understood. In order to study the properties of the media in and around the seismic region, we installed two temporal broadband seismometers near the aftershock area. Using seismic waves recorded just after the mainshock, we analyzed the "*S*-wave splitting" both inside and outside the aftershock region.

S-wave splitting is a phenomenon that an *S*-wave in anisotropic medium splits into two orthogonal polarized waves and propagates with different velocities (Crampin, 1978). The *S*-wave splitting is characterized by two parameters: polarization direction of the fast split *S*-wave and delay time of the slow one. Studies on the *S*-wave splitting in the crust have been done in various regions (e.g. Kaneshima, 1990), and those splitting parameters are contributed to the studies on physics of the crust (e.g. Crampin, 1994). Crampin *et al*. (1980) have suggested that one possible cause of *S*-wave splitting in the crust is the presence of aligned crack system due to the current stress field. Shih and Meyer (1990) found a strong variation of anisotropy in Long Valley Caldera from the polarization direction and the normalized delay times, and indicated the relation of the variation of anisotropy with caldera and magma injection. Saiga *et al*. (2003) found a temporal variation of delay times consistent with the change in the Coulomb failure function (ΔCFF) in the Tokai area in Japan.

Recently, using dense seismic array data or seismic waveforms recorded above the fault, anisotropy in the fault region has been analyzed (e.g. Buchbinder, 1990; Gledhill, 1991; Zhang and Schwartz, 1994; Li, 1996; Li *et al*., 1998). Cochran *et al*. (2003) found a spatial variation of delay times along the fault strike of the Hector Mine fault zone and indicated that delay times are greater in the higher slip area. Tadokoro *et al*. (1999) and Tadokoro and Ando (2002) presented lateral and temporal variation of *S*-wave polarization directions in and around the fracture zone of the 1995 Hyogo-ken Nanbu earthquake, Japan. Mizuno *et al*. (2001) discussed the presence of fluids in the fault system of the 1995 Hyogo-ken Nanbu earthquake from the analysis of *S*-wave splitting using borehole seismometers. In the aftershock region just after the mainshock, cracks are sometimes concentrated so intensive as to affect seismic waves as anisotropy. Analyzing *S*-wave splitting in aftershock area is one of powerful tools to estimate subsurface features there, such as the orientation and the concentration of cracks. In

*Now at: Tono Research Institute of Earthquake Science, Yamanouchi Akeyo-cho 1-63, Mizunami 509-6132, Japan.

Table 1. Summary of stations.

Station name	Latitude (°N)	Longitude (°E)	Altitude (km)	Observation period	Number of identified *S*-wave splitting events
FKB	35.2583	133.3993	0.25	Oct. 8– Dec. 1, 2000	57† (252‡)
RFJ	35.2020	133.4475	0.30	Oct. 8– Dec. 1, 2000*	8† (34‡)

*: RFJ is the trigger type record from October 8 to October 18, 2000.
†: The number of events with δt more than 20 ms and C_{coef} more than 0.8.
‡: The total number of events of M2.0 to 3.5 recorded with high S/N ratio and θ less than 35°.

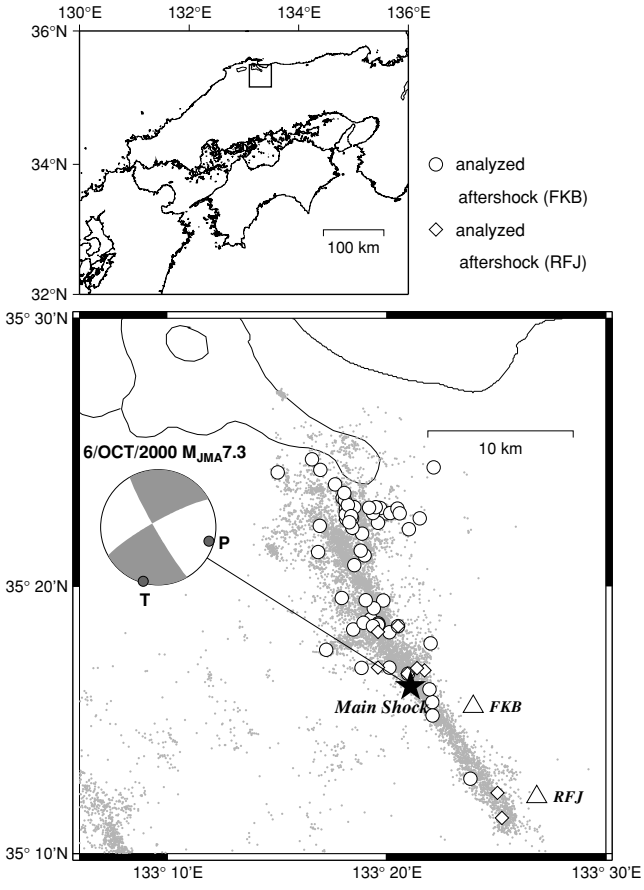

Fig. 1. Epicentral distribution (Japan Meteorological Agency) of the mainshock (star) and aftershocks (shadow) of the 2000 Tottori-ken Seibu earthquake. Two triangles show the seismic stations FKB and RFJ. Open circles and diamonds show the epicenters of aftershocks analyzed in this study for FKB and RFJ, respectively. The focal mechanism (National Research Institute for Earth Science and Disaster Prevention) of the mainshock is also shown.

the present study, we focus on delay times of *S*-wave splitting due to the presence of cracks in and around the aftershock region of the 2000 Tottori-ken Seibu earthquake and examine the spatial variation of anisotropy to reveal the subsurface features associated with the seismic activity.

2. Observation and Data Selection

We conducted aftershock observation at two temporal stations FKB and RFJ (Fig. 1 and Table 1) near the aftershock area to investigate the property of the medium inside and outside it, by using broadband seismographs from October 8 to December 1, 2000 (Nakamura *et al.*, 2002). At station FKB seismic waves were recorded continuously during the observation period. At RFJ data were acquired by trigger system from October 8 to 18 and continuously from October 18 to December 1. At each station a three component velocity-type seismometer VSE11/12 with a flat frequency response from 0.025 to 70 Hz was installed on the hard rock site. The orientation of each seismometer was measured with an accuracy of less than 1 degree using a fiber optic gyro (Watanabe *et al.*, 2000). Waveform data were recorded at a sampling rate of 100 Hz by the datalogger LS-8000WD. By this observation we obtained many records of aftershocks occurring at the depth less than 15 km and at epicentral distance less than 30 km. We selected waveform data for *S*-wave splitting analysis based on the following conditions.

First we picked up the events of M_{JMA}2.0 to 3.5 whose *S*-wave records have high S/N. 453 events were selected at FKB and 230 at RFJ. Among these records, we chose the records with clear initial phase of *S*-waves. Then the number of events becomes 276 for FKB and 36 for RFJ.

Secondly we selected the seismic waves whose incident angles θ are less than 35 degrees, corresponding to the "shear-wave window" of Booth and Crampin (1985) to avoid the influence of *SP* converted wave at the free surface (Evans, 1984). To estimate the incident angle θ, we referred the almost constant V_P/V_S ($\sim$1.70) model of the upper crust of the JMA2001 velocity model (Ueno *et al.*, 2002). We assumed that the incident angle θ of *S*-wave is the same as *P*-wave. We then calculated θ from the direct *P*-wave amplitude ratio between radial and vertical components (e.g., Ben-Menahem and Singh, 2000, equation (3.10); Udias, 1999, equation (5.132)–(5.133); Utsu, 2001, equation (3.78)). After excluding the events whose incident angle is more than 35°, we finally obtained 252 events at FKB and 34 at RFJ for the analysis of *S*-wave splitting. Some examples of the finally selected records are shown in Fig. 2.

3. Analysis of *S*-wave splitting

S-wave splitting is characterized by two parameters: the fast *S*-wave polarization direction (ϕ) and the delay time (δt). The parameter ϕ is the direction of the fast *S*-wave polarization and δt is the difference of the arrival time between the fast and slow *S*-waves. Those parameters are

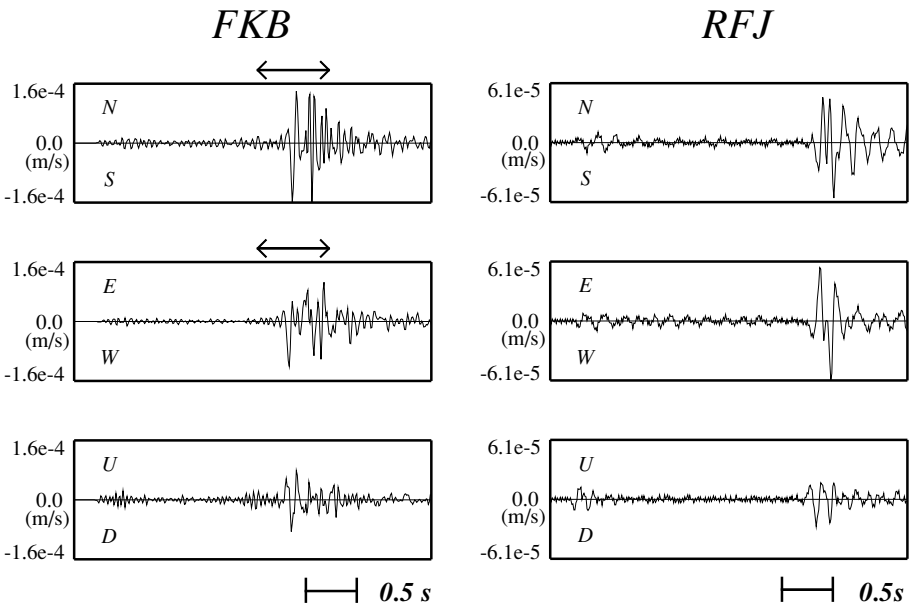

Fig. 2. Examples of seismic waves recorded at FKB (left) and RFJ (right). The arrow portion of FKB is enlarged in Fig. 3(a).

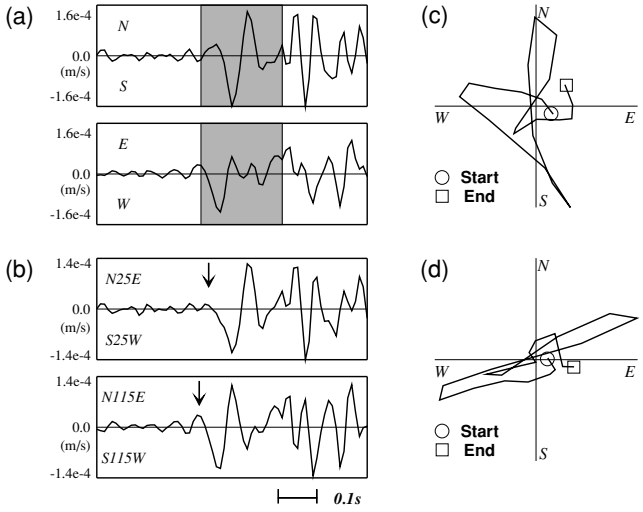

Fig. 3. Example of *S*-wave splitting observed at FKB. The waveform data is the same one in Fig. 2. (a) Waveforms in the components of NS and EW. The shadow zone is the time window used for the cross-correlation calculation. (b) Rotated waveforms of which the cross-correlation coefficient within the time window becomes maximum. The upper and lower figures show waveforms projected in the slow polarization direction (N25°E) and the fast direction (N115°E) of split *S*-waves, respectively. An arrow indicates the onset of *S*-wave. (c) Horizontal particle motion of the seismic wave within the time window. (d) Horizontal particle motion of the records time-shifted with the estimated arrival time difference between the fast and slow *S*-waves.

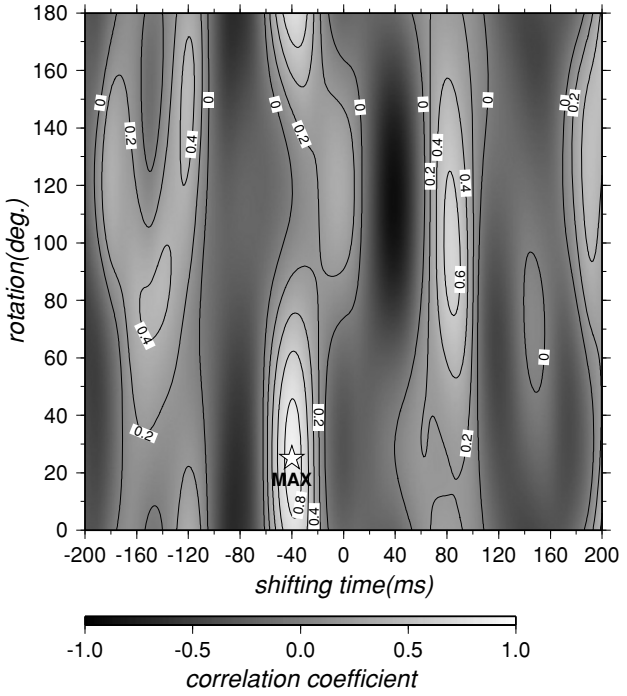

Fig. 4. Contour mapping of the cross correlation coefficient of the waveform within the time window shown in Fig. 3(a). The maximum cross correlation coefficient C_{coef} is 0.89 when the rotation is 25° and the shifting time −40 ms. These values corresponds to ϕ = N115°E and δt = 40 ms, respectively.

estimated using a cross-correlation method (Bowman and Ando, 1987). The cross-correlation method gives ϕ and δt when the cross-correlation coefficient C_{coef} of the two horizontal components becomes maximum in the time window after coordinate rotation and time shift. The cross-correlation coefficient C_{coef} is given by

$$C_{\mathrm{coef}} = \frac{\sum_i (x_i - \bar{x})(y_i - \bar{y})}{\sqrt{\sum_i (x_i - \bar{x})^2 \sum_i (y_i - \bar{y})^2}}, \qquad (1)$$

where x_i and y_i are the amplitudes of the two horizontal components. The values of $\bar{x}$ and $\bar{y}$ are the average amplitudes of x_i and y_i in the time window, respectively. For calculation, the horizontal waveforms in the time window are rotated from 0° to 180° clockwise in a step of 0.5° and shifted with time lags from +200 ms to −200 ms at an interval of 10 ms.

Figure 3(a) shows an example of *S*-wave splitting analy-

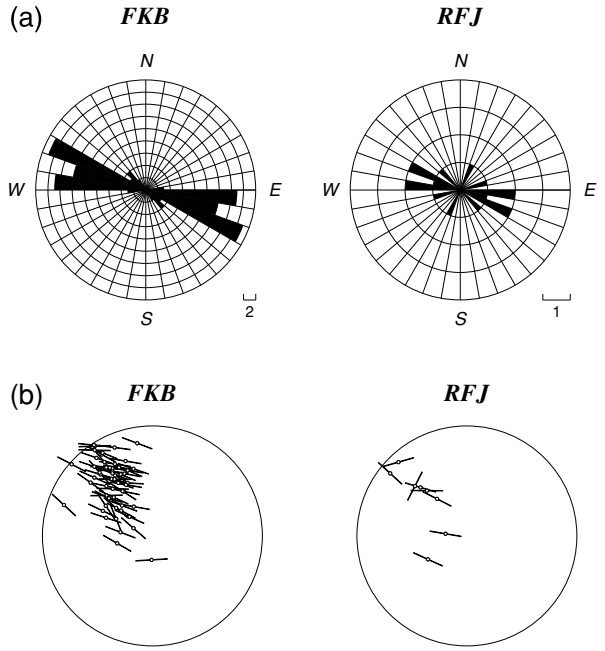

Fig. 5. Polarization directions ϕ of *S*-wave splitting for the stations of FKB (left) and RFJ (right). (a) Rose diagrams of ϕ. (b) Distributions of ϕ in a lower hemi-sphere.

sis. We see a pair of clear phases of splitting with different arrival times in N25°E and N115°E directions (Fig. 3(b)), which are mutually perpendicular in the horizontal plane (Fig. 3(c)). The shadow zone in Fig. 3(a) is the time window used for the calculation. Figure 4 shows the distribution of C_{coef} for various time shifts and rotation angles. In this case, C_{coef} within the time window becomes maximum ($C_{\mathrm{coef}} = 0.89$) at shifting time of -40 ms and coordinate rotation of N25°E, which corresponds to $\delta t = 40$ ms and $\phi =$ N115°E, respectively. Time-shifting the records with this δt, we can see a linear particle motion as shown in Fig. 3(d). In the present study we introduce the following criteria for *S*-wave splitting: C_{coef} is more than 0.8 and δt is more than 20 ms. The latter criterion comes from the minimum resolution of δt (10 ms). The number of events that we successfully estimated the *S*-wave splitting parameters is 57 for FKB and 8 for RFJ (Table 1). The locations of these events are shown in Fig. 1.

4. Results

Figures 5(a) and 5(b) show the estimated polarization directions of ϕ and their distribution in a half sphere, respectively. The mean values of ϕ align N110°E±15° at FKB and N95°E±31° at RFJ, respectively. The distributions of ϕ at both stations show almost the same direction as the *P*-axis (N105°E) obtained from the focal mechanism of the mainshock determined by the NIED (Fig. 1). The measured δt ranges between 20 and 100 ms. Note that the minimum value of δt is 20 ms. In Fig. 6(a) δt is plotted as a function of its back azimuth (measured clockwise from the north in degrees).

To evaluate the degree of anisotropy we introduce the normalized delay time ${}^*\delta t$. The normalized delay time ${}^*\delta t$ is defined as $\delta t/L$ where L is the path length from the source to the station. We measure the path length L from the *S*–*P* time (T_{SP}) of the waveform data. By referring the almost constant $V_P/V_S = 1.70$ model (Ueno *et al.*, 2002), we compute T_S from the T_{SP} and estimate the value of ${}^*\delta t (= \delta t/(T_S V_S))$ from T_S and V_S (=3.531 km/s at 10 km depth in the JMA2001 model). Figure 6(b) shows the values of ${}^*\delta t$ at FKB and RFJ. The mean values of ${}^*\delta t$ at FKB and RFJ are 2.28 ms/km and 2.49 ms/km, respectively.

5. Discussion

The obtained ϕ is dominant along the direction of the *P*-axis of the mainshock (Figs. 1 and 5). This polarization directions of the fast *S*-waves is almost the same as the maximum principal stress direction N107°E in the aftershock area from the stress tensor analysis (Fukuyama *et al.*, 2003). Crampin (1978) proposed that stress induces an anisotropic medium due to a systematic alignment of cracks along the maximum principal stress direction, and the fast *S*-wave is polarized along this direction. Following this idea, a probable main reason for this polarization may be explained by the alignment of cracks by the regional tectonic stress around the aftershock area.

The fast *S*-wave polarization parallel to the fault strike, associated with the shear fractures, is found in some earthquakes but a few. In the aftershock area of the 1995 Hyogoken Nanbu earthquake, Tadokoro *et al.* (1999) observed this type of polarization at the stations just above the fault zone, but did not observe at the stations more than 1 km away from the fault zone. Our stations were not located on the fault zone and there are few events with the polarization direction parallel to the fault strike (Fig. 5). Thus, the main cause of the anisotropy we observed may be due to the presence of cracks created by the tectonic stress and not due to the fracture in the fault zone.

Next, we discuss on the distribution of the normalized delay time ${}^*\delta t$ to the back azimuth. Although the values of δt are not so long comparing with other areas in Japan (e.g., Kaneshima, 1990), ${}^*\delta t$ has a dependence on the back azimuth (Fig. 6(b)). ${}^*\delta t$ at FKB proportionally decreases toward 360° back azimuth, and ${}^*\delta t$ changes drastically around the back azimuth of 330° (dashed line in Fig. 6(b)). The mean value of ${}^*\delta t$ is 1.29 ms/km for the back azimuth above 330°, while below 330° it is 2.72 ms/km. This back azimuth direction of 330° is shown with the aftershock distribution in Fig. 7. It should be noted that the rays mainly pass through the aftershock area when the back azimuth is less than 330° at FKB. This means that ${}^*\delta t$ inside the aftershock region is longer than that outside. In the case of RFJ, we could see a similar feature as at FKB. ${}^*\delta t$ changes sharply around 310° back azimuth (dashed line in Fig. 6(b)), and the mean value above 310° is 1.59 ms/km and below 310° is 4.40 ms/km. ${}^*\delta t$ tends to be longer for the events with longer propagating distance inside the aftershock region (Figs. 6(b) and 7).

In order to confirm the relationship between ${}^*\delta t$ and the aftershock region, we investigated ${}^*\delta t$ using the path fraction R which is defined as the ratio of the propagation distance inside the aftershock region to the total path length. We roughly draw the eastern edge of the aftershock area from the epicenter distribution of aftershocks as shown in

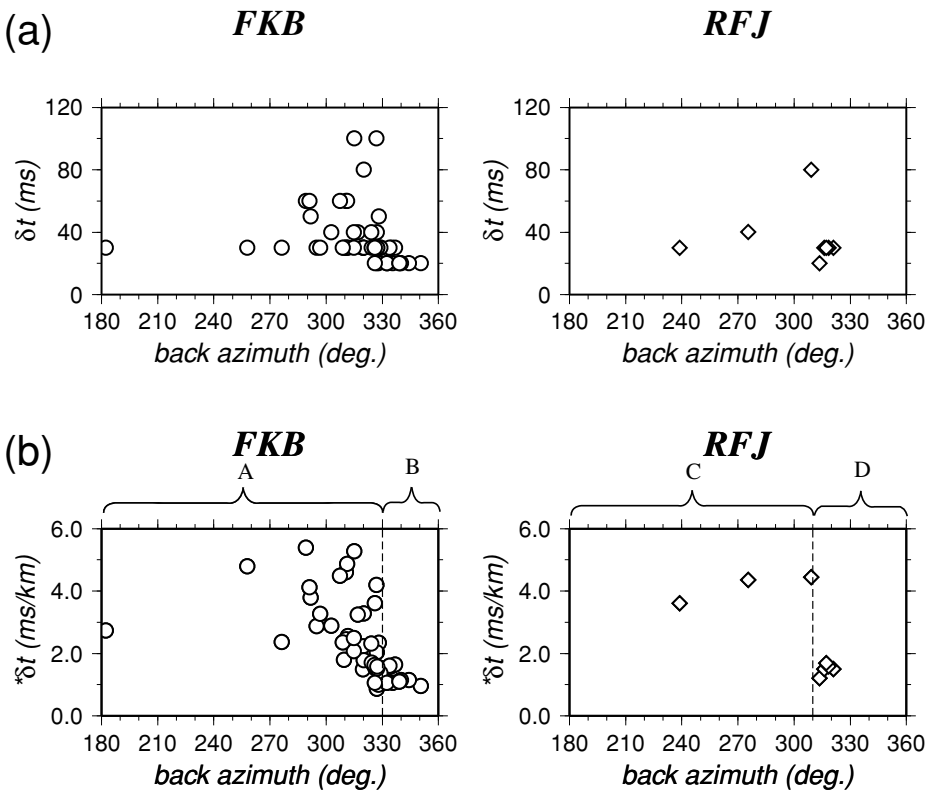

Fig. 6. (a) Delay time δt (upper) and (b) normalized delay time $^*\delta t$ (lower) as a function of back azimuth for station FKB (left) and RFJ (right). Open circles and diamonds show the events with δt more than 20 ms as *S*-wave splitting for FKB and RFJ, respectively. Note that the values of $^*\delta t$ in Figure (b) changes remarkably around broken line. The values $^*\delta t$ in area A (less than 330° back azimuth) in FKB and area C (less than 310° back azimuth) in RFJ are lager than B and D, respectively.

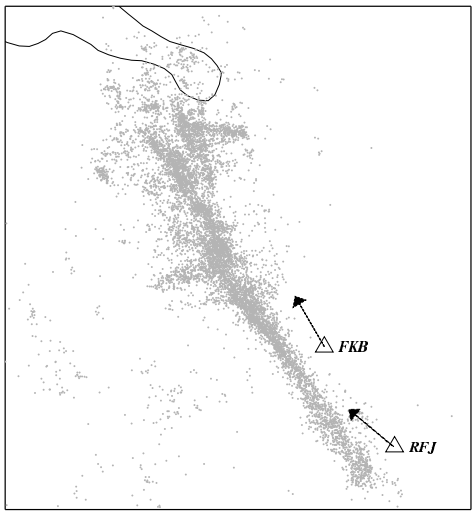

Fig. 7. Directions corresponding to the back azimuth indicated by dashed line in Fig. 6(b).

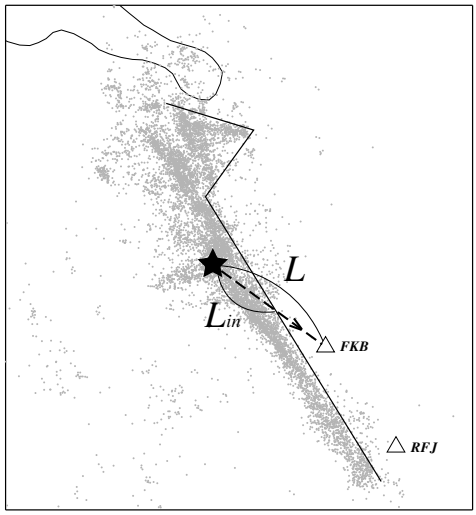

Fig. 8. Schematic illustration of $L_{\rm in}$ and L with eastern edge of the aftershock area we defined in the present study. An example of the epicenter is shown by a solid star. The broken line shows the ray path to the station FKB.

Fig. 8 and we assume this edge as the boundary between inside and outside the aftershock region. We then calculate the ratio R from the locations of event, station, and this aftershock boundary. The ratio of R is given by

$$R = L_{\rm in}/L, \tag{2}$$

where $L_{\rm in}$ is the path length only inside the aftershock region (Fig. 8). The denominator L indicates the whole path length from event to station as defined in the previous section. In the case of $R = 1$, for example, all the *S*-wave propagation paths are inside the aftershock region, while in the case of $R = 0$ the *S*-wave does not propagate inside the aftershock region at all. Using $^*\delta t$ and R for each event, we investigated the dependence of $^*\delta t$ on R. Figure 9 shows the

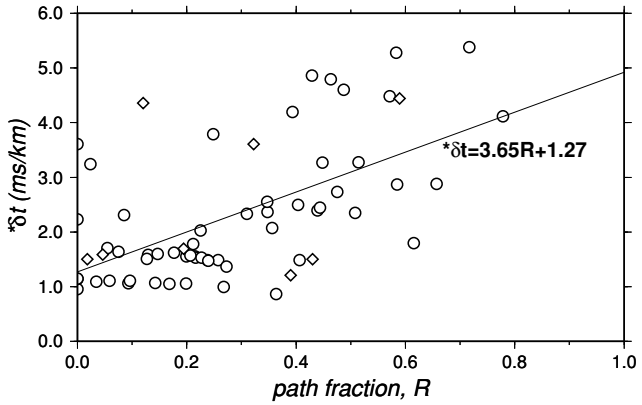

Fig. 9. The normalized delay time $^*\delta t$ as a function of the path fraction R. A regression line is also shown. Symbols are the same as in Figs. 1 and 6.

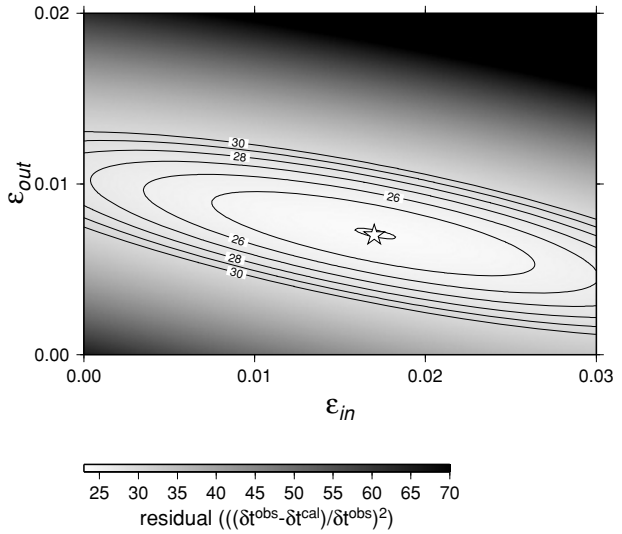

Fig. 10. Contour mapping of the residuals between the observed $\delta t^{\rm obs}$ and the calculated $\delta t^{\rm cal}$ for crack densities of inside $\varepsilon_{\rm in}$ and outside aftershock region $\varepsilon_{\rm out}$. The minimum value of residual (star) between them is at $\varepsilon = 0.017$ for inside region and 0.007 for outside.

relationship between $^*\delta t$ and R with a regression line which has a positive correlation with 0.59 coefficient. This correlation value may depend on the position of the eastern edge of the aftershock region, and actually it is difficult to determine this location precisely enough because of the complex configuration of the fault system. However, the correlation between $^*\delta t$ and R is stable and is always positive even if we set the eastern edge 1 km shifted to the east or west which is comparable to or more than the estimation errors of the epicenter locations. This positive correlation may indicate that the large $^*\delta t$ region tends to exist inside the aftershock area and the small $^*\delta t$ region corresponds to outside the aftershock area. From the right ($R = 1$) and left end points ($R1 = 0$) of this regression line in Fig. 9, the mean value of $^*\delta t$ inside the aftershock region is around 4.92 ms/km, while the mean value outside this region is around 1.27 ms/km. This indicates that the value of $^*\delta t$ inside the aftershock region is about a few times higher than that of the outside.

In order to estimate the degree of anisotropy inside and outside the aftershock region in more detail, we calculated the theoretical delay times $\delta t^{\rm cal}$ based on the Hudson's (1981) crack model for fluid-filled aligned vertical cracks using the crack density ε (O'Connell and Budiansky, 1974). The value of $\varepsilon (= Na^3/V)$ is described by the number of cracks N with radius a in volume V and indicates the degree of anisotropy due to the crack systems. Hudson (1981) showed that the split S-wave velocities as a function of ε and the angle φ between the propagation direction and the normal direction to crack plane can be expressed as follows:

$$V_{S1}{}^2(\varphi, \varepsilon) = V_{S0}{}^2[1 - \frac{16}{3}\varepsilon\frac{\lambda + 2\mu}{3\lambda + 4\mu}\cos^2\varphi], \quad (3)$$

$$V_{S2}{}^2(\varphi, \varepsilon) = V_{S0}{}^2[1 - \frac{16}{3}\varepsilon\frac{\lambda + 2\mu}{3\lambda + 4\mu}(\cos^2\varphi - \sin^2\varphi)^2], \quad (4)$$

where λ and μ are the Lamé constants of host medium. V_{S0} is the S-wave velocity in the isotropic host medium, and V_{S1} and V_{S2} are S-wave velocities split through the medium with cracks ($V_{S1} > V_{S2}$ for the case of incidence nearly perpendicular to the normal of the crack plane). We assume that crack planes are oriented parallel to the P-axis direction of the mainshock (N105°E) and that V_{S0} is 3.531 km/s from the JMA2001 model at the depth of 10 km. Using Eqs. (3) and (4), we can then estimate the theoretical delay time $\delta t^{\rm cal}$ as a function of φ and ε as follows:

$$\delta t^{\rm cal}(\varphi, \varepsilon_{\rm in}, \varepsilon_{\rm out}) = L(|\frac{R}{V_{S1}(\varphi, \varepsilon_{\rm in})} - \frac{R}{V_{S2}(\varphi, \varepsilon_{\rm in})}| + |\frac{1-R}{V_{S1}(\varphi, \varepsilon_{\rm out})} - \frac{1-R}{V_{S2}(\varphi, \varepsilon_{\rm out})}|), \quad (5)$$

where $\varepsilon_{\rm in}$ and $\varepsilon_{\rm out}$ are the crack densities inside and outside the aftershock region, respectively. Minimizing residuals between $\delta t^{\rm cal}$ in Eq. (5) and the observed $\delta t^{\rm obs}$ (=δt in Fig. 6(a)) by a grid search technique, we estimated $\varepsilon_{\rm in}$ and $\varepsilon_{\rm out}$ (Fig. 10). The grid search yields that the values of $\varepsilon_{\rm in}$ and $\varepsilon_{\rm out}$ are 0.017 and 0.007, respectively. These values have significant difference between inside and outside the aftershock region. The crack density ε inside the aftershock area ($\varepsilon_{\rm in} = 0.017$) is about 2 to 3 times higher than that of the outside ($\varepsilon_{\rm out} = 0.007$).

Although ε is not rigorously defined with its physical meaning, it relates the number and the size of cracks or the pores. We therefore propose two major reasons for the spatial variation of crack density ε associated with the aftershock region. First, the existence of high concentration of cracks extending inside the aftershock region is one of the candidate reasons for the high degree of anisotropy there. In the aftershock region, many cracks, including highly damaged material such as fractured rocks, might be brought by before and after the mainshock. Mamada and Takenaka (2004) have found significantly large $Q_{\rm s}^{-1}$ ($Q_{\rm s}$: quality factor of S-wave) in the aftershock region of the 1997 northwestern Kagoshima earthquakes. They pointed out that the attenuation of S-wave inside the aftershock region is several times larger than that outside, indicating concentration of cracks or highly damaged rocks in the aftershock region including the fault zone. Hence, it is reasonable to assume

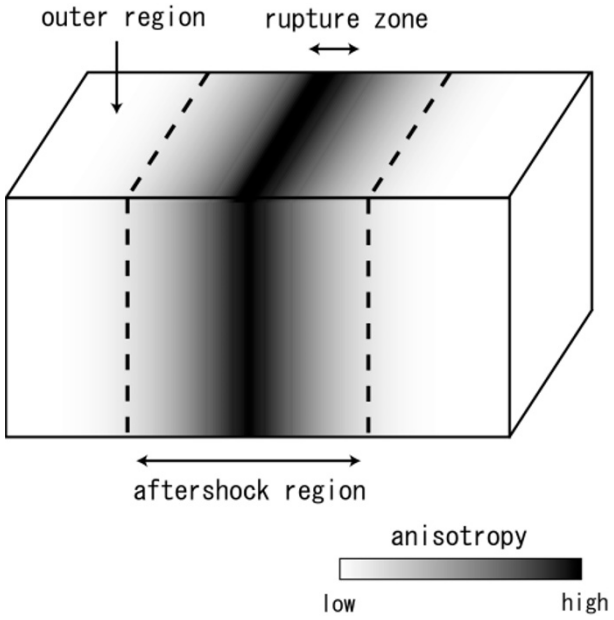

Fig. 11. Schematic illustration of the distribution of the degree of anisotropy and the aftershock region.

that the high concentration of cracks inside the aftershock region is appropriate for the high degree of the anisotropy. Secondly, the high fluid saturation of cracks is also the possible candidates for spatial variation of ε. The existence of the fluid may change the fault strength and even the recurrence intervals of earthquakes (Sibson, 1992), and their behavior in and around the fault zone has been recognized as an important part on the process of faulting or seismic activity (Hickman *et al*., 1995). Ohmi and Obara (2002) have found low frequency earthquakes in the lower crust beneath the mainshock and Oshiman (2002) have pointed out conductivity anomalies in this region, suggesting the existence of fluids, from the electric conductivity study. Zhao *et al*. (2004) have investigated the velocity structure by 3-D tomography in the epicentral area and suggested the appearance of fluids in the upper crust. From the results of these studies in this area, spatial variation of ε in our results may be explained by the existence or immigration of fluids to the aftershock region. In the 1995 Hyogo-ken Nanbu earthquake region Zhao and Mizuno (1999) have estimated the saturation rate of cracks and showed the existence of fluids with high saturated ratio in and below the seismogenic region. Figure 11 shows the schematic illustration in and around the aftershock region we suppose. The degree of anisotropy is high inside the aftershock region associated with the high concentration of cracks or high saturated cracks and will decrease in proportion to the distance from the aftershock region or the rupture zone.

The difference of ε dependent on the aftershock area in our results may be attributed to the existence of highly damaged medium and/or high fluid saturation of cracks as compared with those outside the aftershock area. The study on the spatial variation of the anisotropy around the aftershock area may be one of the key issues to understand earthquake generating processes and an important subject in the future.

6. Conclusion

We conducted aftershock observation at two broadband stations close to the aftershock area of the 2000 Tottori-ken Seibu earthquake. We analyzed *S*-wave splitting in the waveform data and measured the fast *S*-wave polarization direction (ϕ) and the delay time (δt) employing the cross-correlation method.

The mean values of ϕ are N110°E at FKB and N95°E at RFJ. This dominant polarized component aligns almost to the *P*-axis of the focal mechanism. We infer that the main cause of these polarizations is the alignment of cracks by the regional tectonic stress. The measured δt ranges between 20 and 100 ms. We found a strong spatial variation of the normalized delay time $^*\delta t$ which is positively correlated to the fraction of path length inside the aftershock region against the whole path length. The crack density ε inside and outside the aftershock region are estimated to be 0.017 and 0.007, respectively, assuming Hudson's (1981) crack model. It may indicate that in the area of high ε the aftershock activity is intense. This significant difference between inside and outside the aftershock region suggests that the aftershock area may have very different mechanical properties from the surrounding medium.

Acknowledgments. We are grateful to Dr. Keiichi Tadokoro and an anonymous reviewer for their constructive comments. Suggestions from Editor Dr. Eiichi Fukuyama are very helpful to improve the manuscript. We used focal mechanisms and moment magnitudes by the National Research Institute for Earth Science and Disaster Prevention (http://www.fnet.bosai.go.jp/freesia/index-j.html). We obtained hypocentral data of the mainshock and aftershocks from the Japan Meteorological Agency. Dr. Atsushi Watanabe helped with installation and maintenance of seismic stations. Mr. Jafar Gandomi Arash and Dr. Sayed Shaban Refaie Moustafa kindly read the manuscript.

References

Ben-Menahem, A. and S. J. Singh, *Seismic Waves and Sources (2nd edition)*, 1102 pp., Dover, New York, 2000.

Booth, D. C. and S. Crampin, Shear-wave polarizations on a curved wavefront at an isotropic free-surface, *Geophys. J. Roy. Astr. Soc*., **83**, 31–45, 1985.

Bowman, J. R. and M. Ando, Shear-wave splitting in the upper-mantle wedge above the Tonga subduction zone, *Geophys. J. Roy. Astr. Soc*., **88**, 25–41, 1987.

Buchbinder, G. G. R., Shear wave splitting and anisotropy from the aftershocks of the Nahanni Northwest Territories, earthquakes, *J. Geophys. Res*., **95**, 4777–4785, 1990.

Cochran, E. S., J. E. Vidale, and Y. G. Li, Near-fault anisotropy following the Hector Mine earthquake, *J. Geophys. Res*., **108**, 2436, doi:10.1029/2002JB002352, 2003.

Crampin, S., Seismic wave propagation through a cracked solid: polarization as a possible dilatancy diagnostic, *Geophys. J. Roy. Astr. Soc*., **53**, 467–496, 1978.

Crampin, S., The fracture criticality of crustal rocks, *Geophys. J. Int*., **118**, 428–438, 1994.

Crampin, S., R. Evans, B. Üçer, M. Doyle, J. P. Davis, G. V. Yegorkina, and A. Miller, Observations of dilatancy-induced polarization anomalies and earthquake prediction, *Nature*, **286**, 874–877, 1980.

Evans, R., Effects of the free surface on shear wavetrains, *Geophys. J. Roy. Astr. Soc*., **76**, 165–172, 1984.

Fukuyama, E., W. L. Ellsworth, F. Waldhauser, and A. Kubo, Detailed fault structure of the 2000 western Tottori, Japan, earthquake sequence, *Bull. Seism. Soc. Am*., **93**, 1468–1478, 2003.

Gledhill, K. R., Evidence for shallow and pervasive seismic anisotropy in the Wellington region, New Zealand, *Geophys. Res*., **96**, 21503–21516, 1991.

Hickman, S., R. H. Sibson, and R. Bruhn, Introduction to special section:

Mechanical involvement of fluids in faulting, *J. Geophys. Res.*, **100**, 12831–12840, 1995.

Hudson, J. A., Wave speeds and attenuation of elastic waves in material containing cracks, *Geophys. J. Roy. Astr. Soc.*, **64**, 133–150, 1981.

Kaneshima, S., Origin of crustal anisotropy: Shear wave splitting studies in Japan, *J. Geophys. Res.*, **95**, 11121–11133, 1990.

Li, Y. G., Shear wave splitting observations and implications on stress regimes in the Los Angeles basin, California, *J. Geophys. Res.*, **101**, 13,947–13,961, 1996.

Li, Y. G., J. E. Vidale, K. Aki, F. Xu, and T. Burdette, Evidence of shallow fault zone strengthening after the 1992 M 7.5 Landers, California, earthquake, *Science*, **279**, 217–219, 1998.

Mamada, Y. and H. Takenaka, Strong attenuation of shear waves in the focal region of the 1997 Northwestern Kagoshima earthquakes, Japan, *Bull. Seism. Soc. Am.*, **94**, 464–478, 2004.

Mizuno, T., K. Yomogida, H. Ito, and Y. Kuwahara, Spatial distribution of shear wave anisotropy in the crust of the southern Hyogo region by borehole observations, *Geophys. J. Int.*, **147**, 528–542, 2001.

Nakamura, T., H. Takenaka, A. Watanabe, Y. Fujii, and S. Suzuki, Aftershock observation in the focal region of the 2000 Western Tottori earthquake, *Sci. Repts., Dept. Earth and Planet. Sci., Kyushu Univ.*, **21**, 49–59, 2002 (in Japanese with English abstract).

O'Connell, R. J. and B. Budiansky, Seismic velocities in dry and saturated cracked solids, *J. Geophys. Res.*, **79**, 5412–5426, 1974.

Ohmi, S. and K. Obara, Deep low-frequency earthquakes beneath the focal region of the *M*w 6.7 2000 Western Tottori earthquake, *Geophys. Res. Lett.*, **29**, doi:10.1029/2001GL014469, 2002.

Ohmi, S., K. Watanabe, T. Shibutani, N. Hirano, and S. Nakao, The 2000 Western Tottori Earthquake—Seismic activity revealed by the regional seismic networks—, *Earth Planets Space*, **54**, 819–830, 2002.

Oshiman, N., Conductivity structure beneath the western part of Japan, *Earth Monthly*, **38**, 82–90, 2002 (in Japanese).

Saiga, A., Y. Hiramatsu, T. Ooida, and K. Yamaoka, Spatial variation in the crustal anisotropy and its temporal variation associated with the moderate size earthquake in the Tokai region, central Japan, *Geophys. J. Int.*, **154**, 695–705, 2003.

Shih, X. R. and R. P. Meyer, Observation of shear wave splitting from natural events: South moat of Long Valley Caldera, California, June 29 to August 12, 1982, *J. Geophys. Res.*, **95**, 11179–11195, 1990.

Sibson, R. H., Implications of fault-valve behavior for rupture nucleation and recurrence, *Tectonophysics*, **211**, 283–293, 1992.

Tadokoro, K. and M. Ando, Evidence for rapid fault healing derived from temporal changes in *S* wave splitting, *Geophys. Res. Lett.*, **29**, doi:10.1029/2001GL013644, 2002.

Tadokoro, K., M. Ando, and Y. Umeda, *S* wave splitting in the aftershock region of the 1995 Hyogo-ken Nanbu earthquake, *J. Geophys. Res.*, **104**, 981–991, 1999.

Udias, A., *Principles of Seismology*, Cambridge University Press, Cambridge, 475 pp., 1999.

Ueno, H., S. Hatakeyama, T. Aketagawa, J. Funasaki, and N. Hamada, Improvement of hypocenter determination procedures in the Japan Meteorological Agency, *Quart. J. Seism.*, **65**, 123–134, 2002 (in Japanese with English abstract).

Umeda, Y., The 2000 western Tottori earthquake, *Earth Planets Space*, **54**, 3–4, 2002.

Utsu, T., *Seismology (3rd edition)*, Kyoritsu Shuppan, Tokyo, 376 pp., 2001 (in Japanese).

Watanabe, A., H. Takenaka, Y. Fujii, and H. Fujiwara, Seismograph orientation at K-NET observatories (2): Oita Prefecture, *Zisin*, **53**, 185–192, 2000 (in Japanese with English abstract).

Zhang, Z. and S. Y. Schwartz, Seismic anisotropy in the shallow crust of the Loma Prieta segment of the San Andreas fault system, *J. Geophys. Res.*, **99**, 9651–9661, 1994.

Zhao, D. and T. Mizuno, Crack density and saturation rate in the 1995 Kobe earthquake region, *Geophys. Res. Lett.*, **26**, 3213–3216, 1999.

Zhao, D., H. Tani, and O. P. Mishra, Crustal heterogeneity in the 2000 western Tottori earthquake region: effect of fluids from slab dehydration, *Phys. Earth Planet. Inter.*, **145**, 161–177, 2004.

T. Nakamura (e-mail: nakamura@geo.kyushu-u.ac.jp), H. Takenaka (e-mail: takenaka@geo.kyushu-u.ac.jp), S. Suzuki (e-mail: suzuki@tries.jp)